Miscible Binary Blends of Poly(ethylene oxide) and Poly(ether sulfone). 2. Real-Time Small-Angle X-ray Scattering Investigation of the Semicrystalline Morphology

G. Dreezen,[†] N. Mischenko,[†] M. H. J. Koch,[‡] H. Reynaers,[†] and G. Groeninckx*[,†]

Department of Chemistry, Laboratory of Macromolecular Structural Chemistry, Catholic University of Leuven (K.U.Leuven), Celestijnenlaan 200F, B-3001 Heverlee, Belgium, and European Molecular Biology Laboratory, Hamburg Outstation, EMBL c/o DESY, Notkestrasse 85, D-22603 Hamburg, Germany

Received November 19, 1998; Revised Manuscript Received April 10, 1999

ABSTRACT: Miscible blends of the crystallizable component poly(ethylene oxide) (PEO) and an amorphous component poly(ether sulfone) (PES) display a double melting behavior. The lower melting endotherm has been attributed to secondary crystallization starting directly after the primary crystallization. The semicrystalline morphology of these PEO/PES blends was studied in detail using synchrotron radiation. Real time small-angle X-ray scattering experiments performed during isothermal crystallization of the PEO/PES blends reveal that secondary crystalline lamellae are formed between the primary lamellae according to the lamellar insertion model. During melting of the secondary lamellae drastic changes occur in the SAXS patterns. On the basis of these observations, a model describing the semicrystalline morphology of PEO/PES blends is proposed. The scattered intensity of PEO/PES blends after the melting of the secondary lamellae is interpreted in terms of a structure factor and a form factor. Model calculations on the form factor of the proposed semicrystalline structure are in agreement with the observed scattering behavior.

Introduction

The melting behavior of binary blends of a crystallizable and an amorphous component often reveals multiple melting endotherms that are assigned to recrystallization and secondary crystallization.[1−3] Homopolymers such as branched polyethylene,[4,5] poly(phenylene sulfide),[6] and poly(ether ether ketone)[7] also exhibit a complex melting behavior which is often related to the semicrystalline morphology of the system.

Miscible blends of poly(ethylene oxide) (PEO) with an amorphous component poly(ether sulfone) (PES) display a double melting behavior. This has been ascribed to both secondary crystallization and recrystallization of the crystallizable component PEO.[8] After primary crystallization of PEO in PEO/PES blends, depending on the blend composition, a secondary crystallization process starts which forms thin lamellae melting at lower temperatures than the initially formed thick lamellae. The crystallization kinetics strongly depends on the amount of the amorphous component PES in the blends, because of the increased blend T_g with increasing PES content. The long period observed in small-angle X-ray experiments increases with the amount of PES, proving interlamellar segregation of the amorphous component during crystallization of PEO.

Blends of PEO with the amorphous component Aramide 34I display a double melting behavior similar to that of PEO/PES blends resulting from the occurrence of secondary crystallization and recrystallization.[9] The amorphous aromatic polyamide has a glass transition temperature of 225 °C similar to that of PES.

The semicrystalline morphology present after the secondary crystallization depends on the location of the secondary lamellae. These lamellae can be formed within new stacks separated from the primary stacks or between the primary lamellae. Time-resolved X-ray scattering experiments have been performed to investigate the morphological changes upon formation or melting of the secondary lamellae. A model of the semicrystalline structure of PEO/PES blends describing the location of secondary lamellae is presented. The validity of this model is supported by theoretical calculations on the X-ray scattering behavior of PEO/PES blends.

Experimental Section

Materials and Blend Preparation. Poly(ethylene oxide) (PEO, poly[oxyethylene], $-[-CH_2-CH_2-O-]_n-$) obtained from UCB (Belgium) with a viscosity-average molecular weight ($\bar{M}_v$) of 17 000 g/mol and a polydispersity of 1.35 was blended with poly(ether sulfone) (PES, poly[oxy(phenylene)sulfonyl(phenylene)], $-[-C_6H_4-SO_2-C_6H_4-O-]_n-$) (trade name Victrex 4800G) produced by Victrex Limited (UK), with $\bar{M}_v$ of 61 000 g/mol and a polydispersity of 1.72. Both components were dried under vacuum at 80 °C for 2 days prior to blending. Blends were prepared by dissolving the components in dimethylformamide to form 10 wt % solutions in weight compositions between 100/0 and 75/25 PEO/PES. The solvent was removed under vacuum, and the blends were dried in a vacuum oven at 70 °C for 2 days. Before every experiment the blends were additionally dried at 60 °C for 12 h. The glass transition temperature of PEO is −60 °C and that of PES 225 °C.

Differential Scanning Calorimetry. Differential scanning calorimetry (DSC) was performed on a Perkin-Elmer DSC-7 using approximately 6 mg of sample. The PEO/PES blends were melted at 70 °C for 5 min and subsequently isothermally crystallized in the DSC or in a Mettler Toledo FP82 hot stage. After crystallization the samples were heated at a DSC scanning rate of 10 °C/min to determine the melting behavior. The crystallinity was determined from the DSC melting curves according to the method of Mathot et al.[10] The crystallinity does not depend on the definition of an arbitrary

* To whom correspondence should be addressed.
[†] Catholic University of Leuven.
[‡] European Molecular Biology Laboratory.

10.1021/ma981800l CCC: $18.00 © 1999 American Chemical Society
Published on Web 05/29/1999

baseline under the melting peak but is obtained by an analyst-independent determination of the transition enthalpy via an area determination with a baseline extrapolated from the melt. The crystallinity as a function of temperature during cooling or heating is determined from

$$X_c(T) = \frac{[A_2 - A_1]_T}{\Delta h(T)} \quad (1)$$

where $[A_2 - A_1]_T$ is the transition enthalpy. The temperature-dependent enthalpy function $\Delta h(T) = h_a(T) - h_c(T)$ is available from the ATHAS databank[11,12] for several types of semicrystalline polymers. The volume crystallinity $\Phi_v(T)$ was calculated from the overall crystallinity $X_c(T)$, measured by DSC using eq 2:

$$\Phi_v(T) = \frac{1}{1 + \frac{1 - X_c(T)}{X_c(T)} \frac{\rho_c}{\rho_a}} \quad (2)$$

where ρ_c and ρ_a are the crystalline and amorphous densities, respectively; for PEO $\rho_c = 1.239$ g/cm^3 [13] and $\rho_a = 1.124$ g/cm^3.[14]

Real-Time Small-Angle and Wide-Angle X-ray Scattering. Synchrotron radiation X-ray scattering experiments were carried out on the double focusing camera X33[15] of the EMBL in HASYLAB on the storage ring DORIS III of the Deutches Elektronen Synchrotron (DESY) at Hamburg using a wavelength of 1.5 Å. Samples with a thickness of 1 mm were sealed between thin aluminum foils. Small-angle X-ray scattering SAXS and wide-angle X-ray diffraction WAXD patterns were simultaneously collected using gas proportional detectors[16] every 12 s during heating experiments at a heating rate of 10 °C/min (i.e., 1 pattern/2 °C). The temperature program maintained using a Mettler Toledo FP82 hot stage mounted in the X-ray beam path is similar to that used in DSC measurements. The s range (scattering vector $s = (2 \sin \theta)/\lambda$, where 2θ is the scattering angle and λ the wavelength) of the WAXD detector was calibrated using benzoic acid and covers the s range between 0.138 and 0.400 Å^{-1}. The distance between the sample and the SAXS linear position-sensitive detector was 400 cm. The SAXS s range was calibrated using rat tail collagen and ranges from $s = 0.002$ to 0.028 Å^{-1}. The SAXS and WAXD intensity curves were normalized to the primary X-ray beam intensity using the signal of an ionization chamber placed in front of the sample. The SAXS data were corrected for background scattering by subtraction of an amorphous sample in the melt state, and the Lorentz correction was applied. The long period L is obtained from the maximum of the Lorentz-corrected SAXS spectra, and the lamellar thickness l_c is directly obtained as

$$l_c = L\Phi_v(T) \quad (3)$$

Results

PEO/PES blends exhibit a temperature- and composition-dependent miscibility. The blends are miscible in the melt state over the whole composition range up to 75 °C and partially miscible above this temperature. The phase diagram is presented in Figure 1. The crystallization curve T_c indicates the highest temperature at which isothermal crystallization of PEO/PES blends occurs within 5 h. The melting curve T_m represents the observed melting points of samples crystallized at 28 °C for very long times (450 h). The blend T_g increases strongly from −60 to 225 °C with increasing amount of amorphous component PES.

Lamellar Insertion or Dual Lamellar Stack Model. After primary crystallization of PEO in blends with a small amount of PES (up to 25 wt %), PEO displays secondary crystallization forming lamellae melting at lower temperatures than the primary ones.

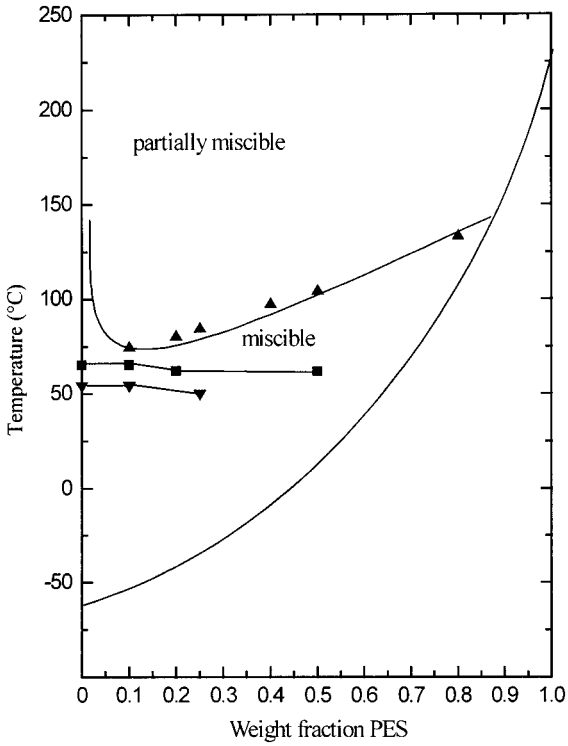

Figure 1. Phase diagram of PEO/PES blends: (▲) cloud point curve, (■) melting temperature T_m, (▼) upper isothermal crystallization temperature T_c, (−) glass transition temperature T_g.

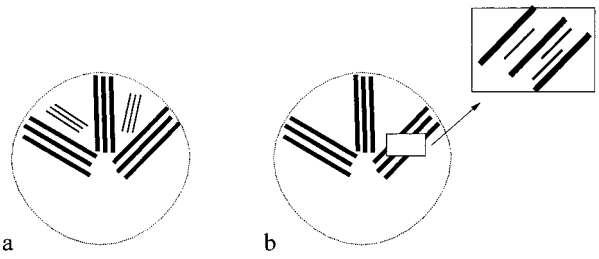

Figure 2. Schematic diagram illustrating (a) the dual lamellar stack model and (b) the lamellar insertion model. Thick lines are primary crystalline lamellae, and thin lines are secondary lamellae.

These secondary lamellae can be formed at different locations in the PEO spherulites as shown schematically in Figure 2. According to the dual lamellar stack model,[17] secondary crystallization results in the formation of stacks of thin lamellae separated from the primary formed lamellar stacks (Figure 2a). In the lamellar insertion model[18,19] the thin secondary lamellae are formed between the thicker primary lamellae within the same stack (Figure 2b). To find out where the secondary lamellae are located within the spherulites, time-resolved small-angle X-ray experiments have been performed. Lorentz-corrected SAXS spectra as a function of the crystallization time of a 75/25 PEO/PES blend isothermally crystallized at 24 °C are shown in Figure 3. DSC melting thermograms of PEO, 85/15, 80/20, and 75/25 PEO/PES blends crystallized at 28 °C for 450 h, and 75/25 PEO/PES blends crystallized at 24 and 34 °C for 60 min are presented in Figure 4. The small lower melting endotherm present between 40 and 50 °C in the DSC curves of the 75/25 PEO/PES blends crystallized at 24 and 34 °C indicates that secondary crystallization starts within 60 min. Soon after the start of the crystallization experiment the SAXS spectra of the 75/

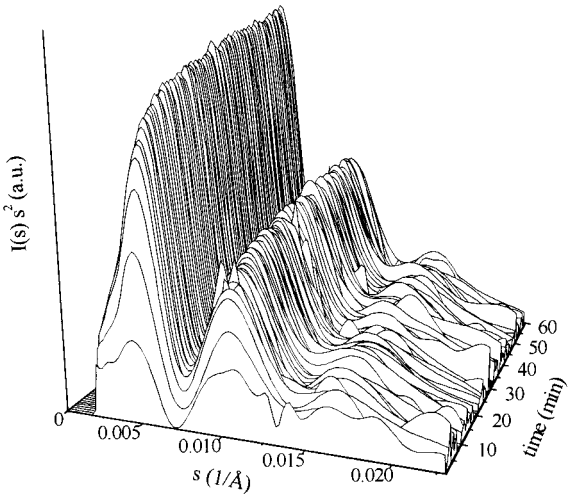

Figure 3. Lorentz-corrected SAXS curves of a 75/25 PEO/PES blends during isothermal crystallization at 24 °C.

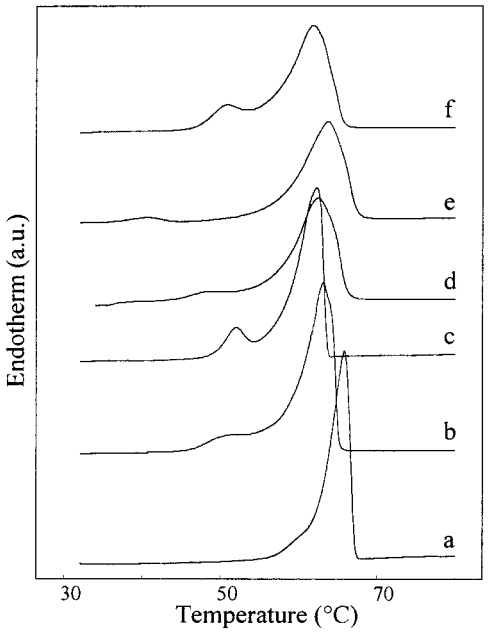

Figure 4. DSC melting curves of PEO/PES blends during heating at 10 °C/min after isothermal crystallization: (a) 100/0, 28 °C, 450 h; (b) 85/15, 28 °C, 450 h; (c) 80/20, 28 °C, 450 h; (d) 75/25, 34 °C, 60 min; (e) 75/25, 24 °C, 60 min; (f) 75/25, 28 °C, 450 h.

25 PEO/PES blend reveal three scattering maxima with periodicity 217, 112, and 57 Å. These correspond to the first three orders of the crystalline repeat in PEO spherulites. Within 60 min no additional scattering maxima appear. If separate stacks of thin lamellae are formed during secondary crystallization, this would result in an additional scattering maximum in the SAXS patterns. In contrast, formation of thin lamellae within the same stack as the primary lamellae would not influence the SAXS pattern. Neither the 75/25 PEO/PES blend crystallized at 24 °C nor any of the other investigated PEO/PES blends showed a clear change in the scattering patterns. The dual lamellar stack model is thus not valid, and one can assume that the secondary lamellae are located between thick primary lamellae according to the lamellar insertion model.

SAXS Behavior of Crystalline PEO/PES Blends during Heating. The secondary lamellae formed during isothermal crystallization melt at lower temperatures than the primary ones. Small-angle and wide-angle X-ray patterns of 85/15, 80/20, and 75/25 PEO/PES blends upon heating were recorded to determine whether the melting of the secondary lamellae, as opposed to their formation, would change the scattering behavior. The SAXS patterns of these blends during heating at a rate of 10 °C/min are shown in Figure 5. The positions of the different scattering maxima are given in Table 1. Figure 5 also contains the scattering patterns of pure PEO crystallized at 28 °C for 450 h. DSC melting curves of these blends are presented in Figure 4.

The 75/25 PEO/PES blend isothermally crystallized at 28 °C for 450 h (Figure 5f) displays SAXS patterns similar to those of the blend crystallized for 60 min at 24 °C (Figure 5e) although there is a small difference in crystallization temperature and a large difference in crystallization time. Clearly, no separate stacks of secondary lamellae are formed after long crystallization times. The long period and the scattered intensity of pure PEO increases during melting; this is attributed to a smaller distribution in lamellar thickness after melting of the smallest lamellae. The SAXS patterns of the PEO/PES blends reveal a remarkable change during heating. Whereas the Lorentz-corrected intensity of the first-order maximum decreases, the intensity of the second order increases starting at temperatures of approximately 45 °C. The DSC thermograms display a double melting behavior. The small lower melting endotherm around 45 °C corresponds to the melting of secondary thin lamellae whereas the primary lamellae melt around 65 °C. Contour plots of the SAXS patterns of the 75/25 PEO/PES blend isothermally crystallized at 24 and 34 °C in Figure 6 clearly illustrate the decrease in intensity of the first-order maximum and the increase in the second-order maximum during heating. Obviously, the observed changes in the scattering patterns are related to the melting of secondary lamellae between 40 and 50 °C.

WAXD spectra during heating of the 75/25 PEO/PES blend isothermally crystallized at 24 and 34 °C are presented in Figure 7. Melting of secondary lamellae does not influence the position of the diffraction peaks in the wide angle region, and the intensity strongly decreases above 60 °C. Apparently the secondary lamellae have the same unit cell as the primary ones but melt at lower temperatures due to differences in lamellar thickness and perfection.

The intensity changes in the SAXS region of the PEO/PES blends are thus related to the melting of thin secondary lamellae located between thick primary ones. Below a model describing the semicrystalline morphology is proposed that allows to explain the observed changes in the SAXS region.

Empirical Model of the Semicrystalline Morphology. Several aspects must be considered before setting up a model for the semicrystalline morphology of 85/15, 80/20, and 75/25 PEO/PES blends. First, during primary crystallization thick PEO lamellae grow which melt around 65 °C. During the secondary crystallization process that starts immediately after the primary crystallization, thinner PEO lamellae melting at lower temperatures are formed between the primary ones, in agreement with the lamellar insertion model. Second, the amorphous component PES segregates interlamellarly during crystallization of PEO. The resulting amorphous PEO/PES phase between the lamellae con-

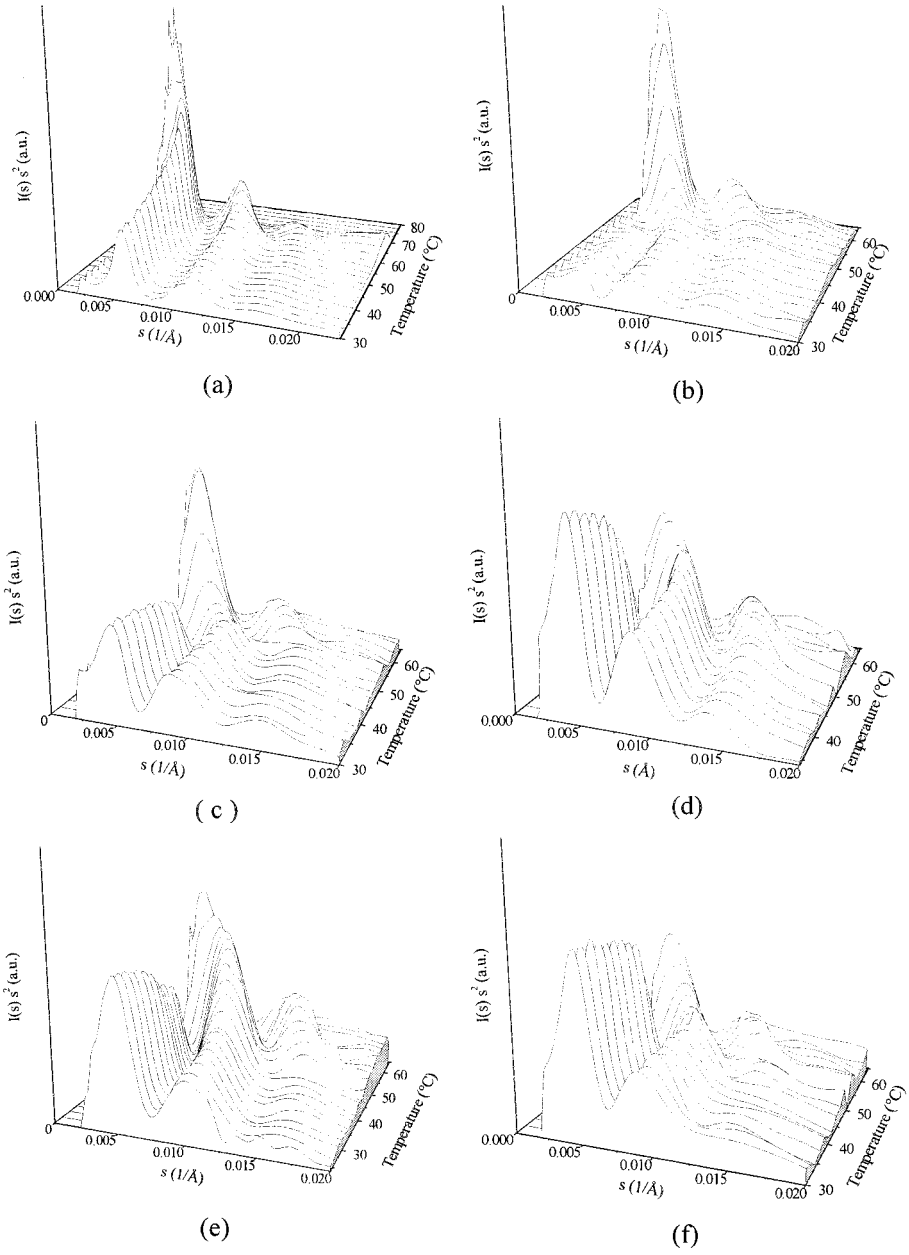

Figure 5. Lorentz-corrected SAXS curves of PEO/PES blends during heating at 10 °C/min after isothermal crystallization: (a) 100/0, 28 °C, 450 h; (b) 85/15, 28 °C, 450 h; (c) 80/20, 28 °C, 450 h; (d) 75/25, 34 °C, 60 min; (e) 75/25, 24 °C, 60 min; (f) 75/25, 28 °C, 450 h. The patterns have been smoothed.

Table 1. Crystallization Conditions and Morphological Parameters of PEO/PES Blends[23]

PEO/PES blend composition	crystallization temp (°C)	L_1 (Å)	L_2 (Å)	L_3 (Å)	$\Phi_v(T_c)$ (%)	$l_c(T_c)$ (Å)	$a(T_c)$ (Å)
85/15	28 °C, 450 h	216	115		80	173	43
80/20	28 °C, 450 h	213	113		72	149	100
75/25	34 °C, 60 min	231	117	70	59	137	94
75/25	24 °C, 60 min	204	101		57	116	88
75/25	28 °C, 450 h	217	112		62	135	82

tains a relatively larger amount of PES, and the glass transition temperature of this amorphous phase is consequently higher than that of the initial blend composition. Third, there is a decreasing concentration gradient of PEO from the crystalline PEO lamellae toward the amorphous PEO/PES phase.

From these mobility and concentration restrictions it is assumed that secondary crystalline lamellae are mainly formed next to the primary ones, rather than in the center between primary lamellae. A model describing the semicrystalline morphology and particularly the location of secondary lamellae between the primary ones is presented in Figure 8a. The morphology of PEO/PES blends consists of thick primary lamellae, thin secondary lamellae next to them, and an amorphous PEO/PES phase. Upon heating at 10 °C/min the secondary lamellae melt first at approximately 40 °C, and the primary ones melt above 55 °C. From the small time delay between these two melting processes (approximately 1.5 min) and the low mobility of the amorphous PEO/PES phase, it is assumed that no homogenization occurs between the molten secondary lamellae and the amorphous PEO/PES phase appears. Consequently, a three-phase structure is present at temperatures between 40 and 55 °C consisting of primary PEO crystals, amorphous PEO (the molten secondary PEO lamellae), and amorphous PEO/PES.

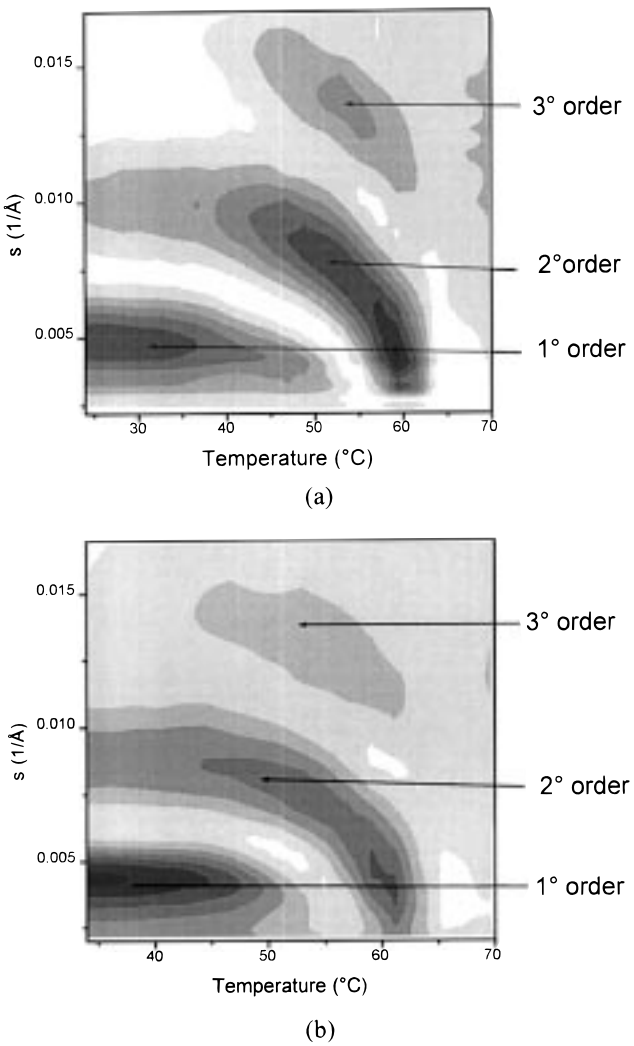

Figure 6. SAXS intensity contour plots of scattering angle versus temperature during heating at 10 °C/min of 75/25 PEO/PES blends isothermally crystallized for 60 min at (a) 24 and (b) 34 °C. Dark areas correspond to high intensities.

Structural Model of the Semicrystalline Morphology. A structural model based on the empirically description of the semicrystalline morphology is presented in Figure 8b. The electron density distribution $\eta(x)$ is expressed as a linear combination of periodic step functions.[20] After melting of secondary lamellae there is a repeating unit with periodicity L consisting of three phases: primary PEO crystalline lamellae with thickness l_c, a miscible amorphous PEO/PES layer with thickness a, and an amorphous PEO layer with thickness $L - l_c - a$.

The total scattered intensity $I(s)$ in the small angle region is given by

$$I(s) \approx F^2(s)\, S(s) \tag{4}$$

where $S(s)$ is the structure factor that leads to maxima in the SAXS curve due to interference of scattering by the periodic repeating unit. $F(s)$ is the form factor of the repeating unit.

The structure factor $F(s)$ is given by the Fourier transform of the electron density function $\eta(x)$ of one period:

$$F(s) = \int_0^L \eta(x) e^{i2\pi sx}\, dx \tag{5}$$

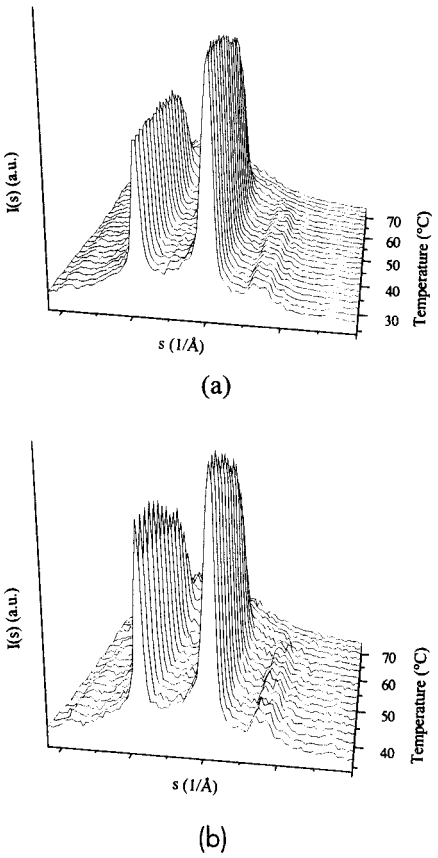

Figure 7. WAXD patterns as a function of temperature during heating at 10 °C/min of 75/25 PEO/PES blends isothermally crystallized for 60 min at (a) 24 and (b) 34 °C. Position of main maxima: $s = 0.223$ Å^{-1} and $s = 0.271$ Å^{-1}.

Placing the origin in the center of the amorphous PEO/PES phase with thickness a makes the system centrosymmetric, and $F(s)$ becomes

$$F(s) = \int_{-L/2}^{L/2} \eta(x) \cos(2\pi sx)\, dx \tag{6}$$

The structure factor $F(s)$ of the model becomes

$$F(s) = 2\left[\int_0^{a/2} \eta(x) \cos(2\pi sx)\, dx + \int_{a/2}^{(L-l_c)/2} \eta(x) \times \cos(2\pi sx)\, dx + \int_{(L-l_c)/2}^{L/2} \eta(x) \cos(2\pi sx)\, dx\right] \tag{7}$$

This can be written as

$$F(s) = 2\frac{1}{2\pi s}\left[\sin\left(\frac{2\pi sa}{2}\right)(\Delta\eta_2 - \Delta\eta_3) + \sin\left(\frac{2\pi s(L - l_c)}{2}\right)(\Delta\eta_3 - \Delta\eta_1) + \sin\left(\frac{2\pi sL}{2}\right)\Delta\eta_1\right] \tag{8}$$

where $\Delta\eta_i = \eta_i - \eta_{av}$ is the contrast and η_1 the electron density of PEO lamellae, η_2 that of the amorphous PEO/PES phase, η_3 that of amorphous PEO, and η_{av} the average electron density in the repeating period calculated from

$$\eta_{av} = \frac{l_c}{L}\eta_1 + \frac{a}{L}\eta_2 + \frac{L - l_c - a}{L}\eta_3 \tag{9}$$

The value of the square of the form factor $F^2(s)$ at the position of first- and second-order interference maximum of the structure factor $S(s)$ was calculated as a

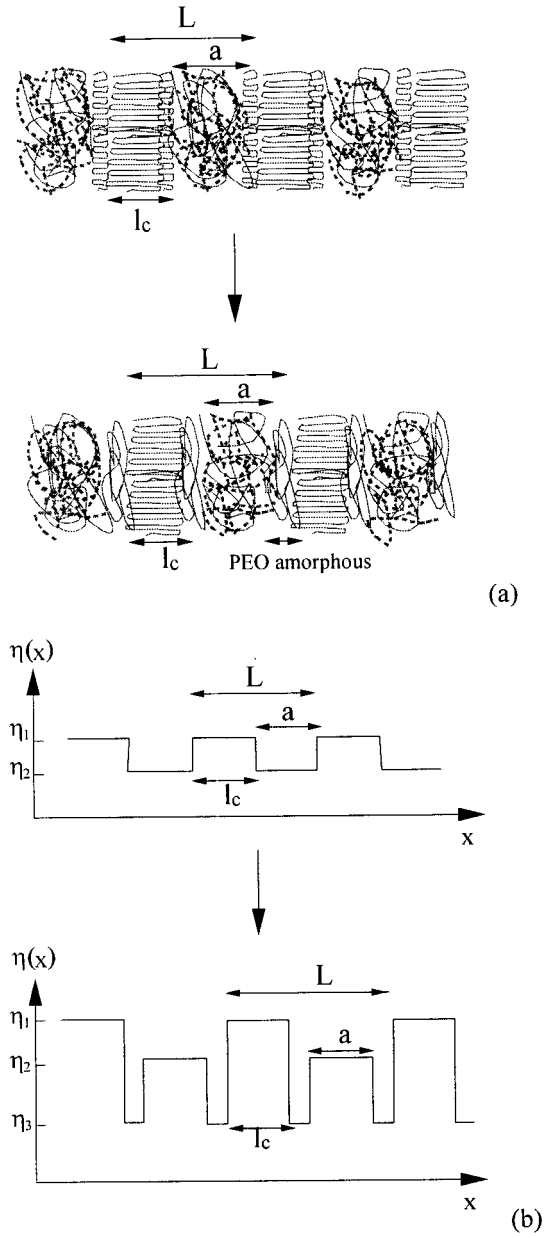

Figure 8. (a) Model describing the semicrystalline morphology of PEO/PES blends before and after melting of secondary lamellae (solid lines, PEO; dashed lines, PES). (b) Electron density profile within the lamellae. L is the long period, l_c the lamellar thickness, a the PEO/PES amorphous layer thickness, η_1 the electron density of PEO lamellae, η_2 the electron density of the miscible amorphous PEO/PES phase, and η_3 the electron density of amorphous PEO.

function of temperature to determine whether changes in the form factor could lead to those observed in the scattered intensity of PEO/PES blends. The form factor $F(s)$ contains six parameters, of which five are well-known: L the experimentally observed repeating unit, l_c the crystal thickness obtained by direct method calculation, a the amorphous PEO/PES layer thickness obtained from $L - l_c$, $\eta_1 = 0.676$ e$^-$ mol/cm^3, and $\eta_3 = 0.612$ e$^-$ mol/cm^3. The electron density η_2 of the amorphous PEO/PES phase is unknown. This parameter was varied between 0.612 and 0.707 e$^-$ mol/cm^3, the electron density of amorphous PEO and PES, in the model calculation.

The long period L, lamellar thickness l_c, amorphous layer thickness a, and crystallinity at the crystallization temperature $\Phi(T_c)$ of the PEO/PES blends are presented in Table 1. When the secondary lamellae start to melt, there is a small increase of the long period L, and as a consequence also the lamellar thickness l_c, obtained by direct analysis, increases. The amorphous PEO/PES layer thickness a is assumed to be constant because of the small time interval for diffusion compared to the low mobility of the PEO/PES amorphous phase The different increase of L and l_c generates a value for the thickness of the amorphous PEO layer obtained from $L-l_c-a$ which is used in the model calculation illustrated in Table 2.

The experimentally determined transition enthalpy $[A_1 - A_2]_T$, the theoretical temperature-dependent enthalpy $\Delta h(T)$ of crystalline PEO,[11,12] and the resulting volume crystalline $\Phi_v(T)$ at different temperatures during the melting of a 75/25 PEO/PES blend crystallized at 24 °C are presented in Table 2 as well. The temperature-dependent enthalpy function $\Delta h(T)$ increases with increasing temperature, and the use of the analyst-independent crystallinity determination function results in higher values for the volume crystallinity from the lower value of $\Delta h(T)$ compared to the often applied thermodynamic enthalpy of fusion at the equilibrium melting temperature (196.4[11,12,21] or 203.3 J/g[22]).

The form factor was calculated as a function of temperature for all the experimentally investigated PEO/PES blends. The square of the form factor versus the scattering angle at different temperatures for a 75/25 PEO/PES blend isothermally crystallized at 24 °C, at an electron density η_2 of 0.657 and 0.688 e$^-$ mol/cm^3, is presented in Figure 9. The model parameters at different temperatures with $\eta_2 = 0.688$ e$^-$ mol/cm^3 are summarized in Table 2. At an electron density $\eta_2 = 0.657$ e$^-$ mol/cm^3, the form factor increases with temperature at all scattering angles from $s = 0$ to 0.013 Å^{-1}. At an electron density η_2 of 0.688 e$^-$ mol/cm^3, the form factor decreases below $s = 0.005$ Å^{-1} and increases from $s = 0.005$ Å^{-1} to $s = 0.013$ Å^{-1} with increasing temperature. This proves that for some values of the electron density η_2 the form factor, and also the scattered intensity, at the second-order maximum can become larger than that at the first-order maximum.

The evolution of the form factor at the first- and second-order scattering maxima as a function of the electron density η_2 of the PEO/PES amorphous phase versus temperature for the 75/25 PEO/PES blend isothermally crystallized at 24 and 34 °C is presented in Figure 10. The dark area indicates the temperature/electron density region where the form factor of the first maximum is larger than that of the second. The light area corresponds to the temperature/electron density region where the form factor of the second-order scattering maximum becomes larger than the first one. During heating, the scattered intensity of a 75/25 PEO/PES blend crystallized at 24 °C becomes larger at the second-order maximum than at the first one above 37 °C. For a 75/25 blend crystallized at 34 °C this occurs from 47 °C. The contour plots in Figure 5 reveal that the change in the SAXS patterns of the 75/25 PEO/PES blend crystallized at 24 and 34 °C starts from 40 and 45 °C, respectively. For values of η_2 between 0.680 and 0.710 e$^-$ mol/cm^3 the model predicts the observed changes in the SAXS patterns fairly well. An overview of the electron density region of the amorphous PEO/PES phase where the form factor predicts the observed scattering behavior is given in Table 3.

Table 2. Parameters Used in the Form Factor Calculation of a 75/25 PEO/PES Blend, Isothermally Crystallized at 24 °C for 60 min

temp (°C)	$[A_1 - A_2]_T$ (J/g)	$\Delta h(T)$ (J/g)	$\Phi_v(T)$ (%)	L (Å)	a (Å)	l_c (Å)	η_1 (e$^-$ mol/cm^3)	η_2 (e$^-$ mol/cm^3)	η_3 (e$^-$ mol/cm^3)	η_{av} (e$^-$ mol/cm^3)
26	99.9	167.7	57.1	204	87	117	0.676	0.688	0.612	0.681
30	101.3	170.5	57.0	207	87	118	0.676	0.688	0.612	0.681
34	102.1	173.3	56.5	210	87	119	0.676	0.688	0.612	0.680
38	102.2	176.0	55.6	213	87	119	0.676	0.688	0.612	0.679
40	101.5	177.4	54.8	213	87	117	0.676	0.688	0.612	0.678
42	100.5	178.7	53.7	223	87	120	0.676	0.688	0.612	0.676
44	100.3	180.1	53.2	230	87	123	0.676	0.688	0.612	0.675
46	100.6	181.4	53.0	242	87	128	0.676	0.688	0.612	0.673
52	99.9	185.3	51.4	262	87	135	0.676	0.688	0.612	0.670
54	98.3	186.6	50.2	279	87	140	0.676	0.688	0.612	0.668

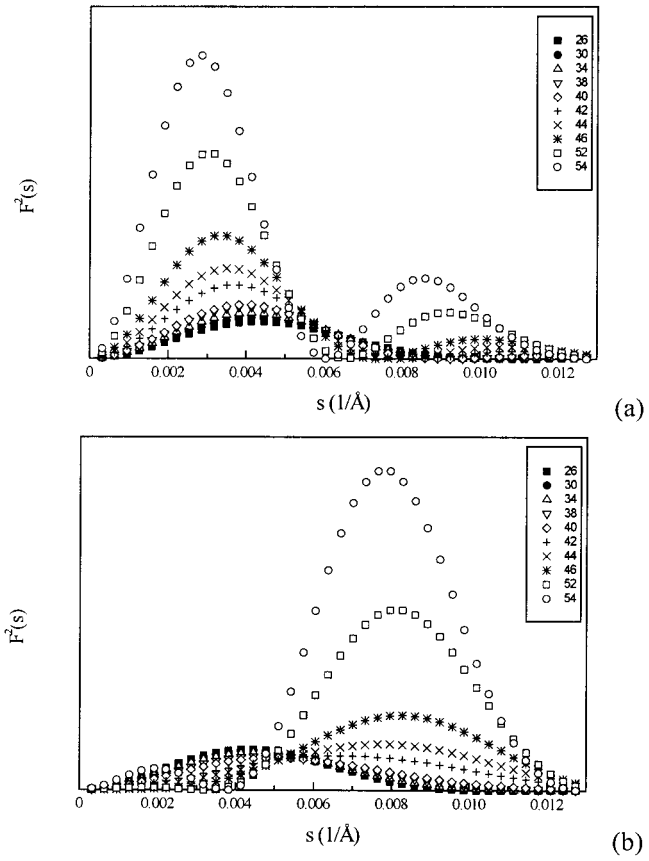

Figure 9. Evolution of the square of the form factor of a 75/25 PEO/PES blend (T_c = 24 °C) with temperature based on different electron densities η_2 of the miscible amorphous PEO/PES phase of (a) 0.657 and (b) 0.688 e$^-$ mol/cm^3.

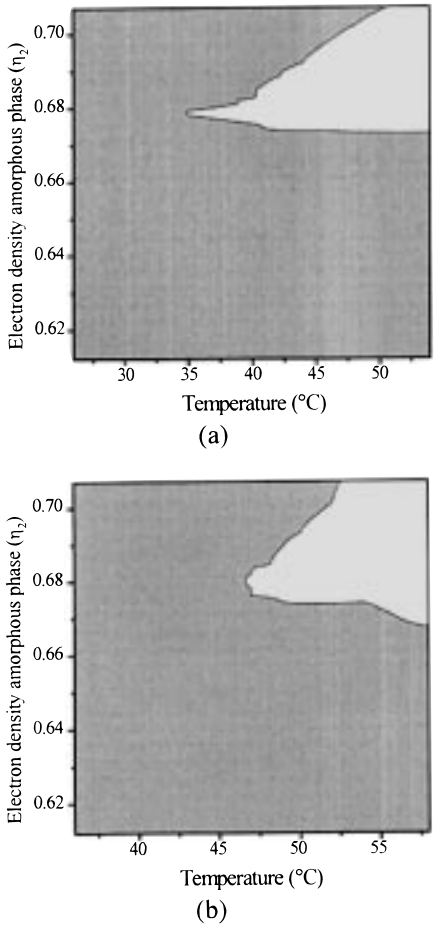

Figure 10. Form factor evolution as a function of electron density and temperature of a 75/25 PEO/PES blend isothermally crystallized for 60 min at (a) 24 and (b) 34 °C. In the dark area, the form factor at the first-order maximum is larger than at the second-order maximum. The situation is reversed in the light areas.

Discussion

The evolution of the form factor of the structural model for PEO/PES blends with increasing temperature predicts the experimentally observed changes in the small-angle X-ray scattering pattern after melting of secondary crystalline lamellae. The model is of course simplified, and it does not account for recrystallization or distributions in the crystalline lamellar and amorphous layer thickness; it uses approximated values for the lamellar and the amorphous layer thickness. One can conclude that the proposed semicrystalline morphology of PEO/PES blends with thin secondary lamellae located next to the thick primary lamellae is reasonable. Similar model calculations on the form factor with the secondary lamellae positioned in the center between the primary ones do not predict the observed behavior and indicate again that the location of the secondary lamellae should be next to the primary ones.

Table 3. Electron Density Region Where the Model Calculation of the Form Factor Fits the Experimental Results of the PEO/PES Blends Studied

PEO/PES blend composition	T_c (°C)	η_2 (e$^-$ mol/cm^3)
85/15	28 °C, 450 h	>0.700
80/20	28 °C, 450 h	0.678−0.700
75/25	34 °C, 60 min	0.674−0.695
75/25	24 °C, 60 min	0.674−0.695
75/25	28 °C, 450 h	0.674−0.700

The specific SAXS scattering behavior is attributed to the high electron density of amorphous PES, which is larger than that of crystalline PEO. The structural model is valid when the electron density of the amorphous PEO/PES phase is higher than that of crystalline

PEO. Blends of PEO with Aramide 34I consist probably of a similar semicrystalline morphology but do not show the specific SAXS behavior.[9] The electron density (0.671 e^- mol/cm^3) of Aramide 34I is smaller than that of PES, and model calculations on this system do not predict changes similar to those in PEO/PES blend.

The model calculations fit the experimental SAXS behavior when the electron density η_2 is above 0.670 e^- mol/cm^3. The glass transition temperature of an amorphous PEO/PES phase with this electron density is approximately 40 °C. This favors our interpretation that secondary lamellae are mainly formed next to primary ones. Secondary crystallization of PEO in the center of the amorphous PEO/PES phase is avoided by the restricted mobility of PEO in this phase.

Conclusions

Secondary crystallization of PEO in a blend with PES occurs between the primary crystalline lamellae, in agreement with the lamellar insertion model. During melting of the secondary lamellae drastic changes occur in the small-angle X-ray scattering behavior of these crystalline PEO/PES blends. A simplified model of the semicrystalline morphology based on the physical properties of the blends (long period and crystallinity of the blends, electron density, and glass transition temperature of the components) can explain these observations. In this model the secondary PEO lamellae are located next to the primary ones, and after melting of the secondary lamellae a three-phase system consisting of primary PEO lamellae, amorphous PEO, and a miscible amorphous PEO/PES phase is obtained. The model calculations indicate that the contribution of the form factor to the scattered intensity results in the observed scattering behavior and gives support to the validity of the proposed semicrystalline morphology model.

Acknowledgment. This research was financially supported by the Research Council K.U.Leuven and the Fund for Scientific Research Flanders (F.W.O-Vlaanderen). G. Dreezen is indebted to the Flemish Institute for the promotion of Scientific-Technological Research in Industry (I.W.T.) for a fellowship. We also thank the European Union for support of the work at EMBL Hamburg through the HCMP Access to Large Installations Project, Contract CHGE-CT93-0040.

References and Notes

(1) Defieuw, G.; Groeninckx, G.; Reynaers, H. *Polymer* **1989**, *30*, 2158.
(2) Defieuw, G.; Groeninckx, G.; Reynaers, H. *Polymer* **1989**, *30*, 2164.
(3) Vanneste, M.; Groeninckx, G. *Polymer* **1994**, *35*, 1051.
(4) Schouterden, P.; Groeninckx, G.; Reynaers, H.; Riekel, C.; Koch, M. H. J. *Polym. Bull.* **1985**, *13*, 533.
(5) Defoor, F.; Groeninckx, G.; Reynaers, H.; Schouterden, P.; Van der Heijden, B. *J. Appl. Polym. Sci.* **1993**, *47*, 1839.
(6) Mai, K.; Zhang, M.; Zeng, H.; Qi, S. *J. Appl. Polym. Sci.* **1994**, *51*, 57.
(7) Crevecoeur, G.; Groeninckx, G. *Macromolecules* **1991**, *24*, 1190.
(8) Dreezen G.; Fang, Z.; Groeninckx, G. *Polymer*, in press.
(9) Dreezen, G.; Koch, M. H. J.; Reynaers, H.; Groeninckx, G. *Polymer*, in press.
(10) Mathot, V. B. F. In *Calorimetry and Thermal Analysis of Polymers*; Mathot, V. B. F., Ed.; Hanser Publishers: Munich, 1994; Chapter 5, pp 105−167, Chapter 9, pp 231−299
(11) Gaur, U.; Lau, S. F.; Shu, H. C.; Wunderlich, B. B. *J. Phys. Chem. Ref. Data* **1983**, *10*, 89, 119, 1001; **1982**, *11*, 313, 1065; **1983**, *12*, 29, 65, 91.
(12) Varma-Nair, M.; Wunderlich, B. B.; Mehta, A. *J. Phys. Chem. Ref. Data* **1991**, *20* (2), 349.
(13) Wunderlich, B. *Macromolecular Physics*; Academic Press: New York, 1973; Vol. 1, p 118.
(14) Wunderlich, B. *Macromolecular Physics*; Academic Press: New York, 1980; Vol. 3, p 67.
(15) Koch, M. H. J.; Bordas, J. *Nucl. Instrum. Methods* **1983**, *208*, 461.
(16) Boulin, C. J.; Kempf, R.; Gabriel, A.; Koch, M. H. J. *Nucl. Instrum. Methods* **1988**, *A269*, 312.
(17) Verma, R.; Marand, H.; Hsiao, B. *Macromolecules* **1996**, *29*, 7767.
(18) Krüger, K.-N.; Zachmann, H. G. *Macromolecules* **1993**, *26*, 5202.
(19) Hsiao, B.; Gardner, K. C.; Wu, D.; Chu, B. *Polymer* **1993**, *34*, 3986.
(20) Takahashi, K.; Miyasaka, K.; Ishikawa, K. *Makromol. Chem.* **1970**, *138*, 37.
(21) Buckley, C. P.; Kovacs, A. J. *Prog. Colloid Polym. Sci.* **1975**, *58*, 44.
(22) Braun, W.; Hellwege, K.-H.; Knappe, W. *Kolloid Z. Z. Polym.* **1967**, *215*, 10.
(23) [a] L_1, L_2, and L_3 correspond to the first, second, and third maximum in the SAXS spectrum; l_c and a are the crystalline and amorphous layer thickness.

MA981800L